minerals

MDPI

Article

# Coupled U–Pb Geochronology of Monazite and Zircon for the Bozhushan Batholith, Southeast Yunnan Province, China: Implications for Regional Metallogeny

**Taotao Yan [1,2,*], Dongsheng Liu [1,2], Chen Si [3] and Yu Qiao [1,2]**

1. Key Laboratory of Geochemical Exploration, Institute of Geophysical and Geochemical Exploration (IGGE), Chinese Academy of Geological Sciences, Langfang 065000, China; liudongsheng@igge.cn (D.L.); qiaoyucugb@163.com (Y.Q.)
2. UNESCO International Centre on Global-scale Geochemistry (ICGG), Langfang 065000, China
3. State Key Laboratory of Geological Processes and Mineral Resources, China University of Geosciences, Beijing 100083, China; 2101170040@cugb.edu.cn

* Correspondence: yantaotao@igge.cn

Received: 7 February 2020; Accepted: 4 March 2020; Published: 6 March 2020

check for updates

**Abstract:** Constraining the duration of magmatism is of vital importance to the understanding of the magmatic-hydrothermal mineral system. The Bozhushan batholith, located in the middle section of the southeastern Yunnan ore district, mainly consists of biotite monzogranite and monzogranite. Many Sn–W–polymetallic deposits are developed around the Bozhushan batholith, but their temporal and genetic relationships remain controversial. LA-ICP-MS U–Pb zircon and monazite dating were respectively conducted on the same two samples, yielding weighted mean $^{206}Pb/^{238}U$ zircon ages of 85.1 ± 0.7 and 85.6 ± 0.9 Ma, and weighted mean $^{206}Pb/^{238}U$ monazite ages of 87.1 ± 0.9 and 88.1 ± 1.1 Ma. The crystallization ages of S-type granites obtained from the zircon U–Th–Pb system and monazite U–Th–Pb system are consistent within the analytical errors. After combining the new ages obtained in this study with recently published U–Pb zircon and cassiterite ages from the giant Baniuchang Ag–Sn–Pb–Zn deposit in the north, and U–Pb zircon and Re-Os molybdenite ages from the large Guanfang W deposit in the south, a temporal framework of magmatism-mineralization in the Bozhushan region has been established. The duration of magmatic activity at Bozhushan is about 7 Ma, with W mineralization occurring at ca. 92 Ma and Sn mineralization at 88–87 Ma.

**Keywords:** monazite; zircon; LA-ICP-MS U–Pb; Bozhushan batholith; southeastern Yunan ore district

---

## 1. Introduction

The southeastern Yunnan ore district, in the western margin of the Cathaysia Block, is famous for hosting abundant Sn, W, Ag, Pb, Zn, and In resources [1–6]. Several world-class Sn–W–polymetallic deposits, such as Gejiu Sn–Cu deposit, Bainiuchang Ag–Sn–Pb–Zn deposit and Dulong Sn–Zn deposit, as well as a series of large deposits to small occurrences, are spatially and genetically associated with Late Mesozoic magmatic activity [1–5]. All of these polymetallic deposits are developed around three Late Cretaceous S-type granitic batholiths that are exposed in the southeastern Yunnan ore district, including Gejiu, Bozhushan, and Laojunshan, which have been proven to be economically important (Figure 1). Among them, the Gejiu and Laojunshan batholiths have been widely investigated and proven to be causative intrusions for the giant Gejiu and Dulong deposit, respectively [7,8]. The giant Bainiuchang deposit is about 15 km northwest of the Bozhushan batholith (Figure 1). This batholith did not attract enough attention until the genetic relationship between recently revealed biotite monzogranite underneath the Bainiuchang deposit and the Bozhushan batholith had been identified [9,10]. However, the duration of magmatic activity in the Bozhushan region remained unclear due to the large discrepancies between previously published age data (whole-rock Rb-Sr: ~115 to 97 Ma [1]; single grain U–Pb age of zircon: 48 Ma [1]; zircon laser ablation-inductively coupled plasma-mass spectrometry (LA-ICP-MS) U–Pb ages: 88 to 85 Ma [4]). Additionally, the large Guanfang W deposit and several Sn–W deposits developed around the Bozhushan batholith [6]. Therefore, more precise ages and a temporal framework of magmatic evolution and associated polymetallic mineralization for the Bozhushan region are required.

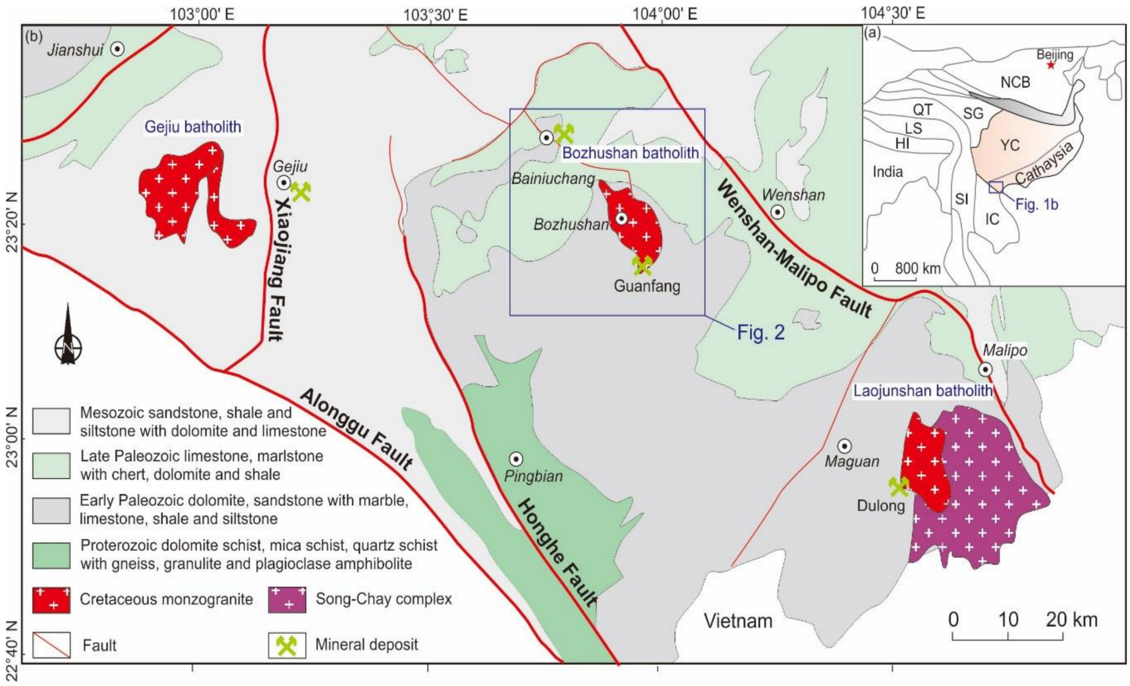


**Figure 1.** (**a**) Geological location of the studied area; (**b**) schematic map of southeastern Yunnan ore district, showing the distribution of Cretaceous batholiths and associated mineral deposits. Abbreviations: HI = High Himalaya Terrane; IC = IndoChina Terrane; LS = Lhasa Terrane; NCB = North China Block; QT = Qiangtang Terrane; SG = Songpan-Ganzi Terrane; SI = Sibumasu Terrane; YC = Yangtze Craton.

Zircon is a highly refractory mineral with relatively low diffusion rates for many elements [11]. It contains relatively high Th and U contents and low common Pb abundances, thus it has a unique U–Th–Pb system and is often used as a mineral to trace magmatism and crustal growth history. Recent studies have shown that monazite also has an effective U–Th–Pb system, which can also be used for dating magmatism, metamorphism and mineralization events [12,13]. Monazite is also characterized by relatively high closure temperatures (700–750 °C) but is significantly more resistant to radiation damage compared with the zircon U–Th–Pb system [14–16]. Notably, monazite is a common mineral phase within S-type granites that crystallizes from metaluminous to peraluminous felsic melts generated by the melting of crustal pelitic composition under a relatively low temperature [17]. Inherited zircons from the host rocks are commonly captured within these granites, making it complex the interpretation of U–Pb zircon ages. In such cases, combining U–Pb monazite ages with zircon ages has been considered as a robust way to constrain the crystallization age of S-type granites [18].

In this study, zircon and monazite U–Pb dating were carried out on the same samples collected from the Bozhushan batholith. These new data were then integrated with recently published geochronological data (U–Pb zircon, Re-Os molybdenite and U–Pb cassiterite) to characterize the specific magmatic processes that led to extensive Sn–W–polymetallic mineralization in the Bozhushan region.

## 2. Geological Setting

### 2.1. Regional Geology

The Bozhushan batholith occurs in the middle section of southeastern Yunnan ore district, adjacent to the Yangtze Craton in the north and to the Sanjiang Tethys Domain to the west (Figure 1). The sedimentary host rocks are dominated by Paleozoic marine-sedimentary rocks consisting of Early Paleozoic siltstone, shale, limestone, and dolomite in the south and Late Paleozoic limestone, marlstone intercalated with chert, dolomite and shale in the northwest. The Mesozoic sedimentary sequence is restricted to the northeast and composed of sandstone, shale, and siltstone intercalated with dolomite and limestone (Figure 2) [19,20]. The most predominant structures in the Bozhushan region are NW-trending and NE-trending faults (Figure 2). The NW-trending faults might have provided conduits for the ascent of magmas, while the NE-trending faults cut the earlier NW-trending faults and the Bozhushan batholith.

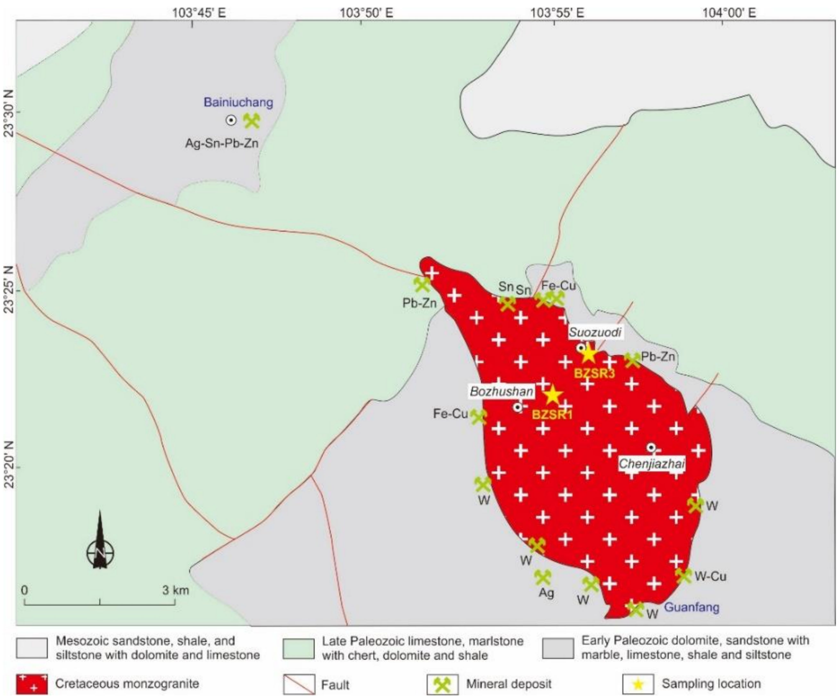


**Figure 2.** Simplified geological map of the Bozhushan Sn–W polymetallic ore district.

Many Sn–W-polymetallic ore deposits/occurrences are distributed around the Bozhushan granitic batholith, such as the Bainiuchang giant skarn Ag–Sn–Pb–Zn deposit, with resources of Ag 6470 t @ 95 g/t, Zn 172 Mt @ 2.46%, Pb 109 Mt @ 1.56% and Sn 8.6 Mt @ 0.12% [21], and the Guanfang skarn W deposit, with resources of W 10 Mt @ 0.5% [6]. The ore-related intrusions of the Bainiuchang deposit, revealed by recent drilling at depths from 1250 to 1420 m, were interpreted to be a branch of the Bozhushan batholith [22,23]. The Bozhushan intrusion was once divided into two-stage phases, including the earlier Chenjiazhai and later Bozhushan phase [1,4], but they have consistent LA-ICP-MS U–Pb zircon ages of 87–86 Ma [4,5], indicating that these granites from the Bozhushan batholith were products of a single magmatic system. The Bozhushan Late Cretaceous granites are alkali-rich, with $K_2O/Na_2O > 1$, A/CNK = molar $[Al_2O_3/(CaO + Na_2O + K_2O)] > 1$, obvious negative Eu anomalies and relatively high whole-rock $(^{87}Sr/^{86}Sr)_i$ ratios of 0.7126 to 0.7257, which are typical values for S-type granites [24]. These S-type granites were formed during the oblique strike-slip motion (89–83 Ma) following the collision between the Okhotomorsk Block and the eastern Eurasia continental margin (100–89 Ma) [5]. The collision was driven by the NW-warding immigration of Paleo-Pacific Plate along the eastern Eurasia continental margin [5,25]. These continuing processes may be responsible for the intense NW-trending faulting and magmatism-mineralization activities in the Bozhushan region [5].

## 2.2. Petrography of Bozhushan Batholith

The Bozhushan batholith is located about 30 km westward away from Wenshan County, Yunnan Province, covering an area of ~120 km$^2$. The rock type is dominated by biotite monzogranite, intruding into the Paleozoic marine-sedimentary rocks along conjunction zone between the NW-trending faults and NE-trending folds (Figure 2). The Bozhushan biotite monzogranite are fine- to medium-grained, with 25–30 vol. % of K-feldspar, 25–30 vol. % of plagioclase, 25–30 vol. % of quartz, and 8–10 vol. % of biotite (Figure 3). Accessory minerals include apatite, zircon, monazite and ilmenite. Samples BZSR1 and BZSR3 were respectively collected from the Bozhushan and Suozuodi area and were used for monazite and zircon LA-ICP-MS U–Pb dating.

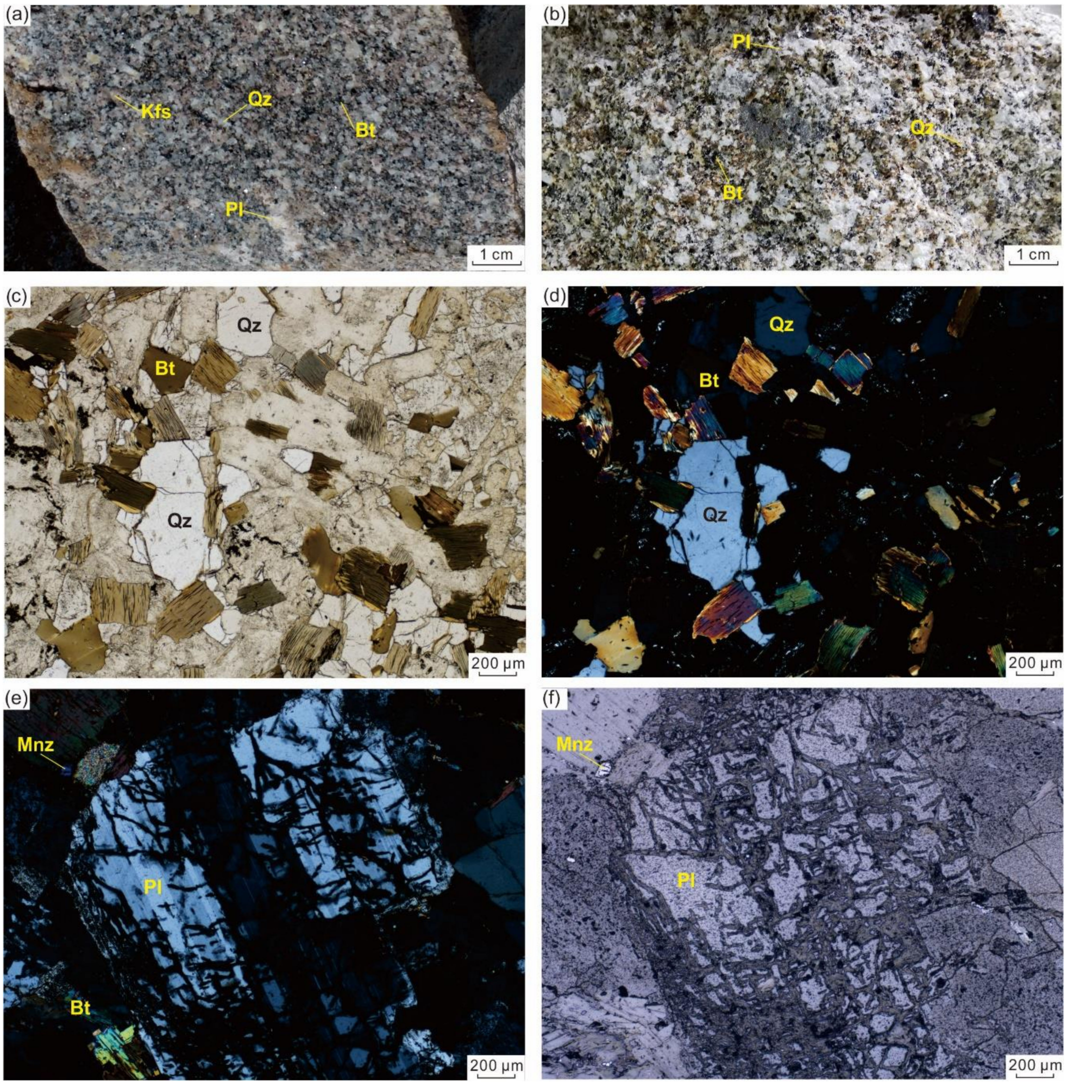


**Figure 3.** (**a**,**b**) representative photographs of hand-specimens from the Bozhushan batholith, showing the fine-medium grained texture of biotite monzogranite. (**c**,**d**) microphotographs of sheeted biotite and paragenetic quartz under plane-polarized light and cross-polarized light. (**d**–**f**) microphotographs of cataclastic plagioclase and intergrown quartz, with interstitial sparse monazite in quartz. Mineral abbreviations: Bt = Biotite; Kfs = K-feldspar; Mnz = monazite; Pl = Plagioclase; Qz = Quartz.

## 3. Analytical Methods

### *3.1. Seperation and Cathodoluminescence Images of Zircon and Monazite*

Zircon and monazite grains were separated by using heavy liquid and magnetic separation techniques at the Langfang Regional Geological Survey, Hebei Province, China. These separated grains were then handpicked under a binocular microscope and examined under transmitted and reflected light in a petrographic microscope. Handpicked zircons were placed on an epoxy mount of 2.5 cm in diameter and polished down to equatorial sections. In order to reveal their internal structures, zircon, and monazite Cathodoluminescence (CL) images were completed using an Analytical Scanning Electron Microscope (JSM-IT100) connected to a GATAN MINICL system at the Wuhan SampleSolution Analytical Technology Co., Ltd., Wuhan, China (SSAT). The imaging condition for zircon was 10 kV voltage of electric field and 80 μA current of tungsten filament, while the imaging condition for monazite was 20 kV voltage and 160 μA current.

### *3.2. In-Situ Zircon LA-ICP-MS U–Pb Dating*

Zircon U–Pb dating and trace element analysis were simultaneously conducted by LA-ICP-MS at the SSAT. For detailed instrument parameters, operating conditions and analysis procedures, as well as data reduction software, please refer to Zong et al. [26]. Laser sampling was performed using a GeolasPro laser ablation system that consists of a COMPexPro 102 ArF excimer laser (Coherent, Santa Clara, CA, USA) (wavelength of 193 nm and maximum energy of 200 mJ) and a MicroLas optical system (Coherent). An Agilent 7700e ICP-MS instrument (Agilent, Santa Clara, CA, USA) was used to acquire ion-signal intensities. During the laser ablation process, helium was used as the carrier gas and argon was used as the compensation gas to adjust the sensitivity. Helium and argon were mixed through a T-connector before entering the ICP. The spot size and frequency of the laser were set to 32 μm and 5 Hz, respectively. Zircon standard 91500 (LA-ICP-MS U–Pb age: 1062 ± 4.0 Ma [27]) and glass NIST610 were applied as external standards for isotopic and trace element fractionation correction, respectively. Eighteen analyses on 91500 collected during sample running returned a weighted mean $^{206}Pb/^{238}U$ age of 1062 ± 5.3 Ma (1σ, 95% confidence). The GJ-1 standard (LA-ICP-MS U–Pb age: 603. 2 ± 2. 4 Ma [28]) was used as a secondary standard to monitor data quality. Six analyses on GJ-1 during the laser session provided $^{206}Pb/^{238}U$ ages varying from 601 to 600 Ma, suggesting that the analytical error is less than 1%. Each time-resolved analysis data includes approximately 20–30 s blank signal and a 50 s sample signal. The off-line processing of analysis data (including the selection of samples and blank signals, the correction for instrument sensitivity drift, element content, U–Pb isotope ratio, and age calculation) was performed using software ICPMSDataCal 11.8 (China University of Geosciences, Wuhan, China) [29,30]. Concordia diagrams and weighted mean calculations of U–Pb zircon ages were made using Isoplot/Ex_ver3 [31]. Common-Pb corrections were made using the method of Anderson [32].

### *3.3. In-Situ Monazite LA-ICP-MS U–Pb Dating*

U–Pb dating and trace element analysis of monazite were also conducted by LA-ICP-MS at the SSAT by using the same laser system. For minerals with relatively high U abundances, a "wire" signal smoothing device was included in the laser ablation system, by which smooth signals are produced, even at very low laser repetition rates down to 1 Hz [33]. It is very useful for in-situ U–Pb dating of high-U mineral [34]. The spot size and frequency of the laser were set to 16 μm and 2 Hz, respectively. Monazite standard 44069 and glass NIST610 were used as external standards for U–Pb dating and trace element calibration, respectively. Reference standard material 44069 (SIMS U–Pb age: 424.9 ± 0.4 Ma [35]) was analyzed after every five unknowns under identical conditions. Sixteen analyses on 44069 collected during sample running defined a weighted mean $^{206}Pb/^{238}U$ age of 425.0 ± 2.1 Ma (1σ, 95% confidence). The Trebilcock standard (LA-ICP-MS U–Pb age: 272 ± 2 Ma [36]) was used as a secondary standard to monitor data quality. Six analyses on Trebilock during laser session have $^{206}Pb/^{238}U$ ages varying from 280 to 274 Ma, indicating that the analytical error is less than 3%. Each analysis incorporated a background acquisition of approximately 20–30 s followed by 50 s of data acquisition from the sample. The $^{207}Pb/^{206}Pb$, $^{206}Pb/^{238}U$, $^{207}Pb/^{235}U$, and $^{208}Pb/^{232}Th$ ratios were calculated from measured ion intensities using ICPMSDataCal 11.8 [28,29]. Concordia diagrams and weighted mean U–Pb ages were processed using Isoplot/Ex_ver3 [29]. Common-Pb corrections were made using the method of Anderson [32].

## 4. Results

### *4.1. Morphology and CL Signatures of Zircon and Monazite*

Zircon grains from two samples (BZSR1 and BZSR3) selected for LA-ICP-MS U–Pb dating are shown in Figure 4a. These zircon crystals are colorless, transparent, and mostly euhedral long-columnar, with lengths of 100–300 μm and length/width ratios of 2:1 to 4:1. Most grains show oscillatory zoning patterns, representing typical features of magmatic zircons. Inherited zircon grains or cores were not found in the samples.

Monazite grains from the same two samples (BZSR1 and BZSR3) selected for LA-ICP-MS U–Pb dating are shown in Figure 4b. The monazite crystals are light-yellow, euhedral to subhedral short-columnar, with lengths of 50–100 μm and length/width ratios of 1:1 to 2:1. Most of monazite grains show homogenous structures and lack oscillatory zoning. Some monazite grains develop corrosion pores within the grains and corrosion rims. In order to obtain more reliable ages for the magmatic evolution, all the analyzed spots in this study avoided these corroded sections.

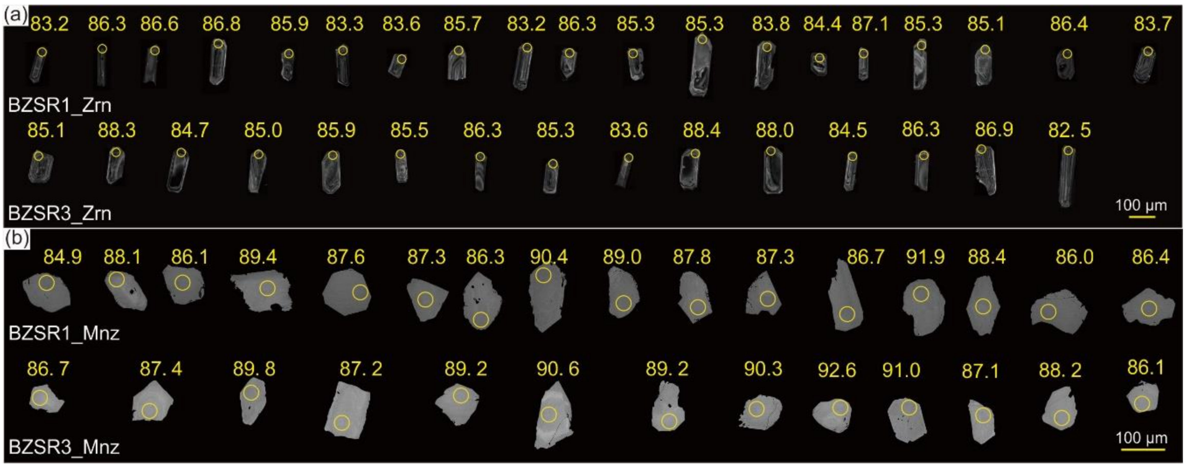


**Figure 4.** Cathodoluminescence (CL) images of analyzed zircons (**a**) and monazites (**b**) from the Bozhushan batholith. Yellow circles and numbers represent the spots selected for laser ablation and the calculated $^{206}Pb/^{238}U$ ages (Ma), respectively.

### *4.2. U–Pb Geochronology of Zircon*

The analyzed U–Pb zircon ages of the Bozhushan batholith are listed in Table 1. Zircon grains from BZSR1 have variable Th (248–1520 ppm) and U (440–2118 ppm) contents, with wide-ranging Th/U ratios of 0.2 to 1.1, suggesting a magmatic origin [37]. Nineteen analyses yielded $^{206}Pb/^{238}U$ ages of 87.1 to 83.2 Ma, with a weighted mean $^{206}Pb/^{238}U$ age of 85.1 ± 0.7 Ma (1σ, MSWD = 2.1; Figure 5a). Zircon grains from BZSR3 have relatively high Th (888–3051 ppm) and U (2843–5270 ppm) contents, with variable Th/U ratios of 0.3 to 1.0. Fifteen analyses yielded $^{206}Pb/^{238}U$ ages ranging from 88.3 to 82.5 Ma, with a weighted mean $^{206}Pb/^{238}U$ age of 85.6 ± 0.9 Ma (1σ, MSWD = 3.0; Figure 5b).

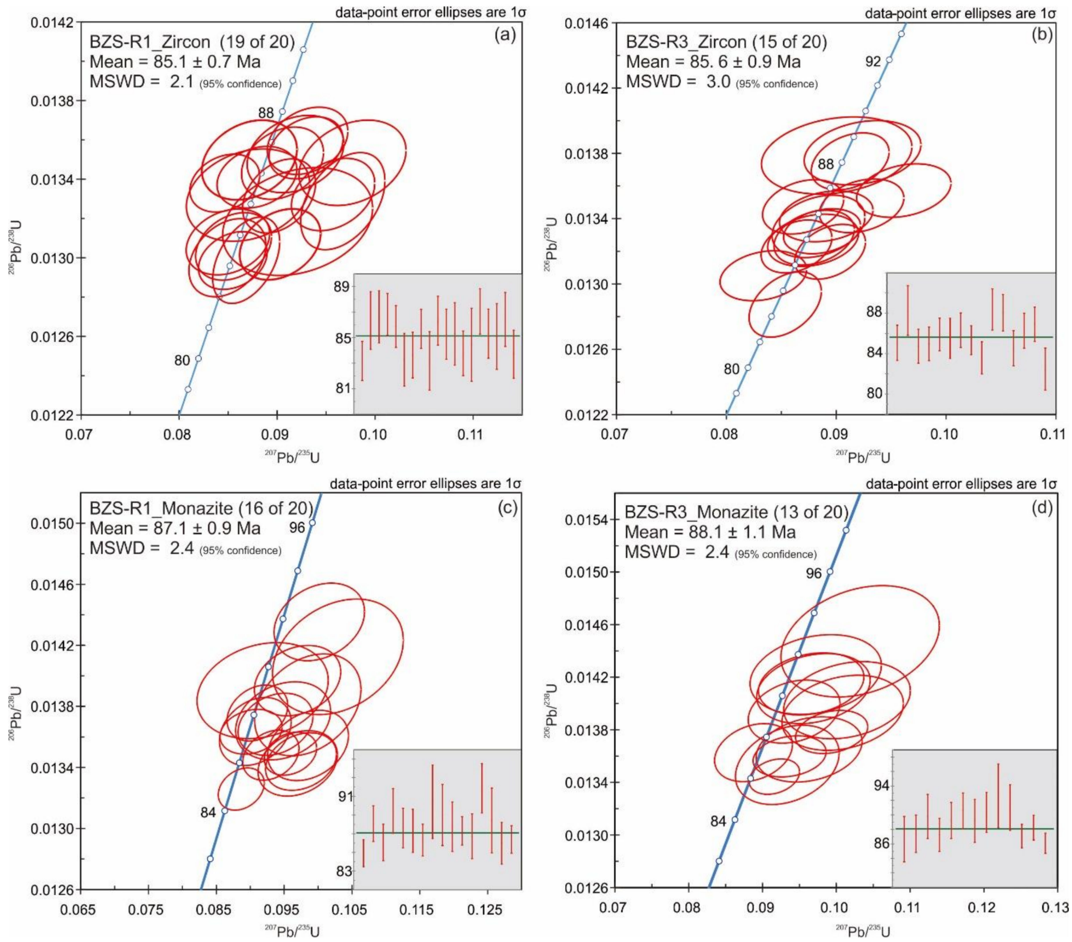


**Figure 5.** (**a**,**b**) LA-ICP-MS zircon U–Pb concordia diagrams for the Bozhushan batholith. (**c**,**d**) LA-ICP-MS monazite U–Pb concordia diagrams for the Bozhushan batholith. The age data and concordia plots were reported at 1σ error, whereas the uncertainties for weighted mean ages are given at a 95% confidence level.

**Table 1.** LA-ICP-MS zircon U–Pb isotopic data of the Bozhusuan batholith.

| Spot No. | Th | U | Th/U | Isotopic Ratios | | | | | Age (Ma) | | | |
|---|---|---|---|---|---|---|---|---|---|---|---|---|
| | (ppm) | (ppm) | | $^{207}$Pb/$^{235}$U | 1σ | $^{206}$Pb/$^{238}$U | 1σ | RHO | $^{207}$Pb/$^{235}$U | 1σ | $^{206}$Pb/$^{238}$U | 1σ |
| BZSR1-01 | 286 | 1597 | 0.2 | 0.0855 | 0.0029 | 0.0130 | 0.0001 | 0.2764 | 83.3 | 2.7 | 83.2 | 0.8 |
| BZSR1-02 | 1204 | 1057 | 1.1 | 0.0977 | 0.0045 | 0.0135 | 0.0002 | 0.2883 | 94.6 | 4.1 | 86.3 | 1.1 |
| BZSR1-03 | 329 | 906 | 0.4 | 0.0919 | 0.0040 | 0.0135 | 0.0002 | 0.2707 | 89.2 | 3.7 | 86.6 | 1.0 |
| BZSR1-04 | 506 | 1682 | 0.3 | 0.0929 | 0.0031 | 0.0136 | 0.0001 | 0.2864 | 90.2 | 2.9 | 86.8 | 0.8 |
| BZSR1-06 | 596 | 1641 | 0.4 | 0.0879 | 0.0033 | 0.0134 | 0.0001 | 0.2526 | 85.6 | 3.1 | 85.9 | 0.8 |
| BZSR1-07 | 469 | 1692 | 0.3 | 0.0849 | 0.0032 | 0.0130 | 0.0002 | 0.3305 | 82.8 | 3.0 | 83.3 | 1.0 |
| BZSR1-08 | 303 | 1144 | 0.3 | 0.0856 | 0.0032 | 0.0131 | 0.0001 | 0.2908 | 83.4 | 3.0 | 83.6 | 0.9 |
| BZSR1-09 | 581 | 1484 | 0.4 | 0.0847 | 0.0029 | 0.0134 | 0.0001 | 0.2619 | 82.5 | 2.7 | 85.7 | 0.8 |
| BZSR1-10 | 1520 | 2118 | 0.7 | 0.0868 | 0.0028 | 0.0130 | 0.0002 | 0.4301 | 84.6 | 2.6 | 83.2 | 1.1 |
| BZSR1-11 | 603 | 1256 | 0.5 | 0.0905 | 0.0034 | 0.0135 | 0.0002 | 0.2955 | 88.0 | 3.2 | 86.3 | 1.0 |
| BZSR1-12 | 1015 | 1644 | 0.6 | 0.0902 | 0.0030 | 0.0133 | 0.0002 | 0.3432 | 87.7 | 2.8 | 85.3 | 1.0 |
| BZSR1-13 | 248 | 1005 | 0.2 | 0.0870 | 0.0051 | 0.0133 | 0.0002 | 0.2440 | 84.7 | 4.8 | 85.3 | 1.2 |
| BZSR1-14 | 525 | 1185 | 0.4 | 0.0850 | 0.0035 | 0.0131 | 0.0001 | 0.2554 | 82.8 | 3.3 | 83.8 | 0.9 |
| BZSR1-15 | 306 | 440 | 0.7 | 0.0921 | 0.0063 | 0.0132 | 0.0002 | 0.2504 | 89.5 | 5.8 | 84.4 | 1.4 |
| BZSR1-16 | 508 | 1507 | 0.3 | 0.0931 | 0.0034 | 0.0136 | 0.0001 | 0.2852 | 90.4 | 3.1 | 87.1 | 0.9 |
| BZSR1-17 | 682 | 1346 | 0.5 | 0.0957 | 0.0035 | 0.0133 | 0.0002 | 0.3112 | 92.8 | 3.2 | 85.3 | 1.0 |
| BZSR1-18 | 944 | 2050 | 0.5 | 0.0967 | 0.0035 | 0.0133 | 0.0002 | 0.4183 | 93.7 | 3.3 | 85.1 | 1.3 |
| BZSR1-19 | 397 | 857 | 0.5 | 0.0872 | 0.0040 | 0.0135 | 0.0002 | 0.2697 | 84.9 | 3.7 | 86.4 | 1.1 |
| BZSR1-20 | 677 | 1284 | 0.5 | 0.0903 | 0.0034 | 0.0131 | 0.0001 | 0.3021 | 87.8 | 3.1 | 83.7 | 0.9 |
| BZSR3-01 | 1234 | 3950 | 0.3 | 0.0880 | 0.0030 | 0.0133 | 0.0001 | 0.3038 | 85.6 | 2.8 | 85.1 | 0.9 |

**Table 1.** *Cont.*

| Spot No. | Th (ppm) | U (ppm) | Th/U | Isotopic Ratios | | | | | Age (Ma) | | | |
|---|---|---|---|---|---|---|---|---|---|---|---|---|
| | | | | $^{207}Pb/^{235}U$ | 1σ | $^{206}Pb/^{238}U$ | 1σ | RHO | $^{207}Pb/^{235}U$ | 1σ | $^{206}Pb/^{238}U$ | 1σ |
| BZSR3-03 | 2160 | 2843 | 0.8 | 0.0900 | 0.0056 | 0.0138 | 0.0002 | 0.2252 | 87.5 | 5.2 | 88.3 | 1.2 |
| BZSR3-05 | 1469 | 4784 | 0.3 | 0.0864 | 0.0026 | 0.0132 | 0.0001 | 0.3281 | 84.1 | 2.5 | 84.7 | 0.8 |
| BZSR3-06 | 888 | 3270 | 0.3 | 0.0879 | 0.0034 | 0.0133 | 0.0001 | 0.2562 | 85.5 | 3.2 | 85.0 | 0.8 |
| BZSR3-07 | 1692 | 3668 | 0.5 | 0.0891 | 0.0035 | 0.0134 | 0.0001 | 0.2425 | 86.7 | 3.2 | 85.9 | 0.8 |
| BZSR3-08 | 1693 | 2968 | 0.6 | 0.0884 | 0.0035 | 0.0134 | 0.0002 | 0.2991 | 86.0 | 3.2 | 85.5 | 1.0 |
| BZSR3-10 | 1333 | 3830 | 0.3 | 0.0923 | 0.0031 | 0.0135 | 0.0001 | 0.2922 | 89.7 | 2.9 | 86.3 | 0.9 |
| BZSR3-11 | 1111 | 3525 | 0.3 | 0.0887 | 0.0029 | 0.0133 | 0.0001 | 0.2616 | 86.3 | 2.7 | 85.3 | 0.7 |
| BZSR3-13 | 1890 | 3086 | 0.6 | 0.0834 | 0.0032 | 0.0131 | 0.0001 | 0.2481 | 81.3 | 3.0 | 83.6 | 0.8 |
| BZSR3-14 | 3051 | 3065 | 1.0 | 0.0924 | 0.0043 | 0.0138 | 0.0002 | 0.2476 | 89.7 | 4.0 | 88.4 | 1.0 |
| BZSR3-15 | 1384 | 3628 | 0.4 | 0.0913 | 0.0029 | 0.0138 | 0.0001 | 0.3271 | 88.7 | 2.7 | 88.0 | 0.9 |
| BZSR3-16 | 1712 | 4042 | 0.4 | 0.0894 | 0.0026 | 0.0132 | 0.0001 | 0.3535 | 87.0 | 2.5 | 84.5 | 0.9 |
| BZSR3-17 | 1355 | 4096 | 0.3 | 0.0870 | 0.0030 | 0.0135 | 0.0001 | 0.2906 | 84.7 | 2.8 | 86.3 | 0.9 |
| BZSR3-18 | 1102 | 4553 | 0.2 | 0.0962 | 0.0035 | 0.0136 | 0.0001 | 0.2706 | 93.2 | 3.2 | 86.9 | 0.9 |
| BZSR3-19 | 1890 | 5270 | 0.4 | 0.0854 | 0.0027 | 0.0129 | 0.0002 | 0.4030 | 83.2 | 2.5 | 82.5 | 1.0 |

### *4.3. U–Pb Geochronology of Monazite*

The analyzed U–Pb monazite ages of the Bozhushan batholith are listed in Table 2. All the monazites are characterized by relatively high Th (1.54–10.43 wt. %) and U (754–9033 ppm) abundances. Sixteen monazites from sample BZSR1 yielded $^{206}Pb/^{238}U$ ages varying from 91.9 to 84.9 Ma, with a weighted mean $^{206}Pb/^{238}U$ age of 87.1 ± 0.9 Ma (1σ, MSWD = 2.1; Figure 5c). Thirteen monazites from sample BZSR3 yielded $^{206}Pb/^{238}U$ ages varying from 92.6 to 86.1 Ma, with a weighted mean $^{206}Pb/^{238}U$ age of 88.1 ± 1.1 Ma (1σ, MSWD = 2.1; Figure 5c).

**Table 2.** LA-ICP-MS monazite U–Pb isotopic data of the Bozhusuan batholith.

| Spot No. | Th (wt.%) | U (ppm) | Isotopic Ratios | | | | | Age (Ma) | | | |
|---|---|---|---|---|---|---|---|---|---|---|---|
| | | | $^{207}Pb/^{235}U$ | 1σ | $^{206}Pb/^{238}U$ | 1σ | RHO | $^{207}Pb/^{235}U$ | 1σ | $^{206}Pb/^{238}U$ | 1σ |
| BZSR1(MZ)-01 | 4.89 | 7565 | 0.0887 | 0.0028 | 0.0133 | 0.0001 | 0.2734 | 86.3 | 2.6 | 84.9 | 0.7 |
| BZSR1(MZ)-02 | 10.43 | 4086 | 0.0911 | 0.0037 | 0.0138 | 0.0001 | 0.2710 | 88.5 | 3.4 | 88.1 | 1.0 |
| BZSR1(MZ)-03 | 6.24 | 4503 | 0.0975 | 0.0043 | 0.0134 | 0.0002 | 0.2616 | 94.5 | 4.0 | 86.1 | 1.0 |
| BZSR1(MZ)-04 | 10.11 | 1879 | 0.0970 | 0.0052 | 0.0140 | 0.0002 | 0.2514 | 94.0 | 4.8 | 89.4 | 1.2 |
| BZSR1(MZ)-05 | 4.20 | 3046 | 0.0937 | 0.0045 | 0.0137 | 0.0002 | 0.2529 | 91.0 | 4.2 | 87.6 | 1.1 |
| BZSR1(MZ)-06 | 6.20 | 2452 | 0.0907 | 0.0043 | 0.0136 | 0.0002 | 0.2801 | 88.2 | 4.0 | 87.3 | 1.2 |
| BZSR1(MZ)-07 | 6.09 | 9033 | 0.0930 | 0.0034 | 0.0135 | 0.0001 | 0.2729 | 90.3 | 3.1 | 86.3 | 0.9 |
| BZSR1(MZ)-08 | 7.38 | 795 | 0.1029 | 0.0079 | 0.0141 | 0.0003 | 0.2863 | 99.5 | 7.2 | 90.4 | 2.0 |
| BZSR1(MZ)-09 | 4.67 | 953 | 0.0918 | 0.0079 | 0.0139 | 0.0003 | 0.2148 | 89.2 | 7.3 | 89.0 | 1.6 |
| BZSR1(MZ)-10 | 8.32 | 3022 | 0.0948 | 0.0057 | 0.0137 | 0.0002 | 0.2528 | 92.0 | 5.3 | 87.8 | 1.3 |
| BZSR1(MZ)-11 | 6.84 | 4041 | 0.0901 | 0.0037 | 0.0136 | 0.0001 | 0.2117 | 87.6 | 3.5 | 87.3 | 0.8 |
| BZSR1(MZ)-15 | 5.24 | 2147 | 0.0985 | 0.0049 | 0.0135 | 0.0002 | 0.2813 | 95.4 | 4.5 | 86.7 | 1.2 |
| BZSR1(MZ)-16 | 6.39 | 1915 | 0.1002 | 0.0055 | 0.0144 | 0.0002 | 0.2659 | 96.9 | 5.0 | 91.9 | 1.3 |
| BZSR1(MZ)-17 | 5.25 | 867 | 0.0985 | 0.0064 | 0.0138 | 0.0003 | 0.3040 | 95.4 | 5.9 | 88.4 | 1.7 |
| BZSR1(MZ)-18 | 5.46 | 3824 | 0.0970 | 0.0048 | 0.0134 | 0.0002 | 0.2650 | 94.0 | 4.4 | 86.0 | 1.1 |
| BZSR1(MZ)-19 | 7.67 | 6793 | 0.0959 | 0.0032 | 0.0135 | 0.0001 | 0.2596 | 93.0 | 2.9 | 86.4 | 0.7 |
| BZSR3(MZ)-01 | 7.03 | 1344 | 0.0934 | 0.0057 | 0.0135 | 0.0002 | 0.2961 | 90.6 | 5.3 | 86.7 | 1.6 |
| BZSR3(MZ)-02 | 1.54 | 2107 | 0.0963 | 0.0059 | 0.0137 | 0.0002 | 0.2437 | 93.4 | 5.4 | 87.4 | 1.3 |
| BZSR3(MZ)-03 | 7.48 | 1207 | 0.1015 | 0.0070 | 0.0140 | 0.0002 | 0.2471 | 98.1 | 6.5 | 89.8 | 1.5 |
| BZSR3(MZ)-04 | 4.90 | 2304 | 0.0888 | 0.0043 | 0.0136 | 0.0002 | 0.2724 | 86.4 | 4.0 | 87.2 | 1.1 |
| BZSR3(MZ)-06 | 4.49 | 1717 | 0.0943 | 0.0051 | 0.0139 | 0.0002 | 0.2611 | 91.5 | 4.7 | 89.2 | 1.2 |
| BZSR3(MZ)-08 | 7.21 | 2345 | 0.0966 | 0.0058 | 0.0141 | 0.0002 | 0.2257 | 93.6 | 5.4 | 90.6 | 1.2 |
| BZSR3(MZ)-10 | 7.57 | 1561 | 0.1009 | 0.0067 | 0.0139 | 0.0002 | 0.2510 | 97.6 | 6.2 | 89.2 | 1.5 |
| BZSR3(MZ)-11 | 5.08 | 1423 | 0.0969 | 0.0063 | 0.0141 | 0.0002 | 0.2378 | 93.9 | 5.8 | 90.3 | 1.4 |
| BZSR3(MZ)-12 | 6.86 | 754 | 0.1032 | 0.0088 | 0.0145 | 0.0003 | 0.2814 | 99.8 | 8.1 | 92.6 | 2.2 |
| BZSR3(MZ)-13 | 4.25 | 1572 | 0.0972 | 0.0073 | 0.0142 | 0.0002 | 0.2327 | 94.2 | 6.7 | 91.0 | 1.6 |
| BZSR3(MZ)-16 | 4.87 | 4464 | 0.0937 | 0.0040 | 0.0136 | 0.0001 | 0.2175 | 90.9 | 3.8 | 87.1 | 0.8 |
| BZSR3(MZ)-18 | 8.32 | 5060 | 0.0994 | 0.0040 | 0.0138 | 0.0001 | 0.2421 | 96.2 | 3.7 | 88.2 | 0.9 |
| BZSR3(MZ)-19 | 5.10 | 7020 | 0.0916 | 0.0028 | 0.0134 | 0.0001 | 0.2682 | 89.0 | 2.6 | 86.1 | 0.7 |

### 4.4. Rare Earth Element Patterns of Zircon and Monazite

Zircons from the Bozhushan batholith exhibit enrichment of heavy rare earth elements (HREEs) relative to light rare earth elements (LREEs), significant positive Ce anomalies and negative Eu anomalies (Figure 6a,b). Monazites are characterized by enriched LREEs and depleted LREEs, with negative Eu anomalies (Figure 6c,d).

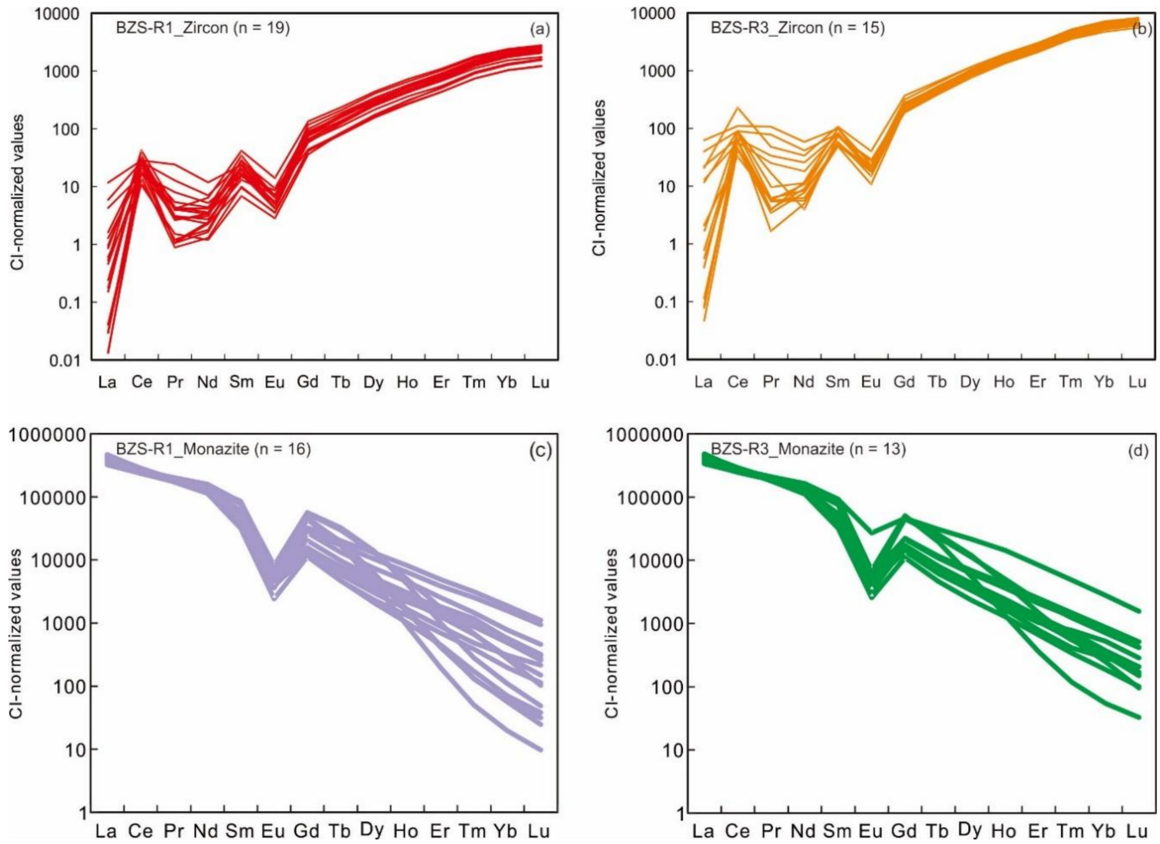


**Figure 6.** (**a**,**b**) Chondrite (C1)-normalized REE distribution patterns of zircon grains from the Bozhushan batholith. (**c**,**d**) C1-normalized REE distribution patterns of monazite grains from the Bozhushan batholith. The elemental abundances of C1 were from [38].

## 5. Discussion

Several Sn–W-polymetallic deposits represented by the giant Bainiuchang Ag–Sn–Pb–Zn deposit and large Guanfang W deposit are spatially and genetically related to the Bozhushan batholith (Figure 2). Previous whole-rock Rb–Sr and single zircon grain U–Pb age data have shown that the Bozhushan batholith was emplaced during the Early Cretaceous to Late Eocene (115–48 Ma) [1]. However, several works reported Late Cretaceous crystallization ages for the Bozhushan batholith and coincident Late Cretaceous mineralization ages (Table 3; Figure 7). Li [20] and Chen et al. [25] reported zircon LA-ICP-MS U–Pb ages of 91 to 86 Ma for granite porphyry and biotite monzogranites obtained from drill holes made in the Bainiuchang deposit, which are consistent with the age spectrum of 92 to 84 Ma yielded by cassiterite LA-ICP-MS U–Pb dating [21]. Biotite monzogranite samples collected from the Bozhushan, Chenjiazhai and Suozuodi batholiths have similar weighted mean zircon $^{206}Pb/^{238}U$ ages varying from 87.8 ± 0.4 to 85.1 ± 0.7 Ma, corresponding to their U–Pb monazite ages of 88–87 Ma obtained in this study. The Guanfang W deposit, hosted at the contacts between the southernmost Bozhushan batholith and a Middle Cambrian marble, has provided a Re-Os molybdenite isochron age of 91.6 ± 1.3 Ma [6]. These molybdenite grains used for dating coexist with scheelite, thus the isochron age could represent the timing of W-dominated mineralization in the Bozhushan region.

Monzogranite and biotite monzogranite samples from the Guanfang area (i.e., the southernmost of Bozhushan batholith) have weighted mean zircon $^{206}Pb/^{238}U$ ages of 91.6 ± 1.0 Ma and 88.6 ± 0.8 Ma, respectively [6,20]. Additionally, Li [20] reported that the SHRIMP U–Pb zircon ages of porphyritic biotite monzogranites in the Guanfang area varies from 89.5 ± 0.4 to 87.3 ± 0.3 Ma, which is consistent with the ages of W-dominated mineralization. The compilation of geochronological data for the Bozhushan batholith and representative deposits demonstrates that both the emplacement of granitic magmas and the extensive Sn–W–polymetallic mineralization occurred during the Late Cretaceous (92–85 Ma). The duration of granitic magmatism in the Bozhushan region revealed by compiled U–Pb zircon and monazite ages is about 7 Ma, with the earlier W-mineralization occurring at ca. 92 Ma and the later Sn-mineralization occurring at ca. 88–87 Ma (Figure 6). The temporal discrepancy between W-mineralization and Sn-mineralization might be a product of a long-lived fertile magmatic-hydrothermal systems that lasted for several million years, in which the highly evolved magmas would be much more favorable to the enrichment in Sn [39].

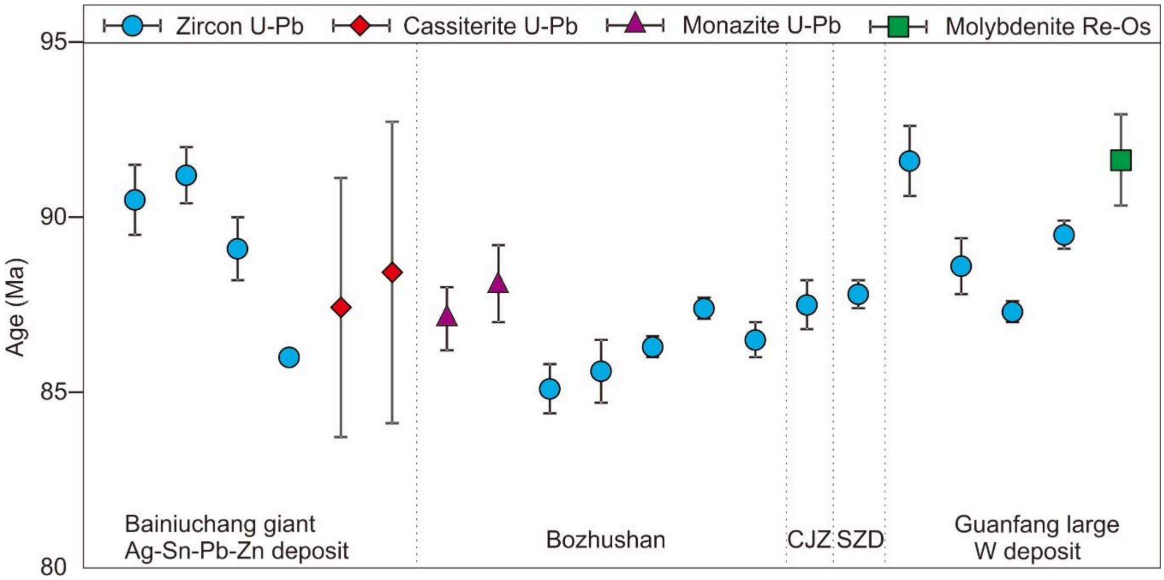


**Figure 7.** Compilation of geochronological data for the Bozhushan batholith and representative deposits, southeastern Yunnan district. Data sources: The Bainiuchang giant Ag–Sn–Pb–Zn deposit is from [20,21,25]; The Bozhushan area is from [4,25]; The Chenjiazhai (CJZ) area is from [4]; The Suozuodi (SZD) area is from [4]; The Guanfang large W deposit is from [6,20].

The Gejiu and Laojunshan batholiths in the southeastern Yunnan ore district have magmatism-mineralization age spectrums of 95–77 Ma [7,40,41] and 93–77 Ma [5,42,43], suggesting that the Late Cretaceous is a period of extensive magmatic activities and associated Sn–W-polymetallic mineralization in the southeastern Yunnan Province. Cheng et al. [5] compared the geological features and geochronological data of Sn–W mineralization in southeastern Yunnan Province with those in northeastern Vietnam, and concluded that they share many similarities and should have formed under the same lithospheric extensional setting in response to the subduction of the Palaeo-Pacific Plate. In summary, the Late Cretaceous granitic rocks in the southeastern Yunnan Province are closely related to Sn–W-polymetallic mineralization, especially at the contacts between these granites and Paleozoic marbles.

**Table 3.** Geochronological data for the Bozhushan batholith and representative deposits, southeastern Yunnan district.

| Region | Rock Type | Sample No. | Method | Age (Ma) | Genetic Type | Metal | Tonnage | Age (Ma) | Method |
|---|---|---|---|---|---|---|---|---|---|
| Bainiuchang | Fine- to medium-grained biotite monzogranite | BN1380–01 | Zircon LA-ICP-MS U–Pb | 90.5 ± 1.0 [20] | Skarn | Ag–Sn–Pb–Zn | 6470 t@95 g/t Ag, 172 Mt@2.46% Zn, 109 Mt@1.56% Pb, 8.6 Mt@0.12% Sn | 87.4 ± 3.7 [21] | Cassiterite LA-ICP-MS U–Pb |
| | Fine- to medium-grained biotite monzogranite | ZK146–05 | Zircon LA-ICP-MS U–Pb | 91.2 ± 0.8 [20] | | | | 88.4 ± 4.3 [21] | Cassiterite LA-ICP-MS U–Pb |
| | Fine- to medium-grained biotite monzogranite | ZK146-N1 | Zircon LA-ICP-MS U–Pb | 89.1 ± 0.9 [20] | | | | | |
| | Granite porphyry | DMS | Zircon LA-ICP-MS U–Pb | 86.0 ± 0.2 [25] | | | | | |
| Bozhushan | Fine- to medium-grained biotite monzogranite | BZS-R1 | Monazite LA-ICP-MS U–Pb | 87.1 ± 0.9 | | | | | |
| | Fine- to medium-grained biotite monzogranite | BZS-R3 | Monazite LA-ICP-MS U–Pb | 88.1 ± 1.1 | | | | | |
| | Fine- to medium-grained biotite monzogranite | BZS-R1 | Zircon LA-ICP-MS U–Pb | 85.1 ± 0.7 | | | | | |
| | Fine- to medium-grained biotite monzogranite | BZS-R3 | Zircon LA-ICP-MS U–Pb | 85.6 ± 0.9 | | | | | |
| | Medium- to coarse-grained biotite monzogranite | BZS-1 | Zircon LA-ICP-MS U–Pb | 86.3 ± 0.3 [25] | | | | | |
| | Medium- to coarse-grained biotite monzogranite | BZS-2 | Zircon LA-ICP-MS U–Pb | 87.4 ± 0.3 [25] | | | | | |
| | Fine- to medium-grained biotite monzogranite | CYB0807079 | Zircon LA-ICP-MS U–Pb | 86.5 ± 0.5 [4] | | | | | |
| Chenjiazhai | Porphyritic biotite monzogranite | CYB0807086 | Zircon LA-ICP-MS U–Pb | 87.8 ± 0.4 [4] | | | | | |
| Suozuodi | Porphyritic biotite monzogranite | CYB0807084 | Zircon LA-ICP-MS U–Pb | 87.5 ± 0.7 [4] | | | | | |
| Guanfang | Medium-grained biotite moznogranite | ZK8–234-01 | Zircon LA-ICP-MS U–Pb | 91.6 ± 1.0 [6] | Skarn | W | 10 Mt@0.5% W | 91.6 ± 1.3 [6] | Molybdenite Re–Os |
| | Fine- to medium-grained monzogranite | HDPD06–01 | Zircon LA-ICP-MS U–Pb | 88.6 ± 0.8 [6] | | | | | |
| | Fine- to medium-grained porphyritic biotite monzogranite | YTS-01 | Zircon SHRIMP U–Pb | 87.3 ± 0.3 [20] | | | | | |
| | Fine- to medium-grained porphyritic biotite monzogranite | YTS-02 | Zircon SHRIMP U–Pb | 89.5 ± 0.4 [20] | | | | | |

**Author Contributions:** T.Y. wrote the paper and performed data reduction; T.Y. formulated the problem and revised paper. D.L., C.S. and Y.Q. provided help during the field work and experiment analysis. All authors have read and agreed to the published version of the manuscript.

**Funding:** This research was funded by the National Nonprofit Institute Research Grant of IGGE (Grant number JY201907) and the Geological Investigation Work Project of China Geological Survey (Grant number DD20190450).

**Acknowledgments:** We would like to thank Qingjie Gong from the China University of Geoscience in Beijing for providing valuable comments on earlier versions of this manuscript. Sincere thanks are extended to Hongfang Chen and Zheng Liu for their help with zircon and monazite U–Pb dating.

**Conflicts of Interest:** The authors declare no conflict of interest.

## References

1. Zhang, S.T.; Chen, C.G. Geological characteristics and evolution rule of Bozhushan complex granite in southeastern Yunnan. *Yunnan Geol.* **1997**, *16*, 222–232, (In Chinese with English abstract).
2. Mao, J.W.; Xie, G.Q.; Guo, C.L.; Chen, Y.C. Large-scale tungsten–tin mineralization in the Nanling region, South China: Metallogenic ages and corresponding geodynamic processes. *Acta Petrol. Sin.* **2007**, *23*, 2329–2338, (In Chinese with English abstract).
3. Xie, H.J.; Zhang, Q.; Zhu, C.H. Petrology and REE-trace element geochemistry of Bozhushan Granite Pluton in Southeastern Yunnan Province, China. *Acta Mineral. Sin.* **2009**, *29*, 481–490, (In Chinese with English abstract).
4. Cheng, Y.B.; Mao, J.W.; Chen, X.L.; Li, W. LA-ICP-MS zircon U–Pb dating of the Bozhushan granite in southeastern Yunnan province and its significance. *J. Jilin Univ. (Earth Sci. Ed.)* **2010**, *40*, 869–878, (In Chinese with English abstract).
5. Cheng, Y.B.; Mao, J.W.; Liu, P. Geodynamic setting of Late Cretaceous Sn–W mineralization in southeastern Yunnan and northeastern Vietnam. *Solid Earth Sci.* **2016**, *1*, 79–88. [CrossRef]
6. Zhang, Y.; Zhang, S.; Tan, S.; Cui, Y.; Zhao, Z.; Jiang, Y.; Jiang, S.; Tao, S. The genetic relationship between the large Guanfang W deposit and granitic intrusions, in Yunnan Province, southwest China: Evidence from U Pb and Re Os geochronology and Pb and Sr isotopic characteristics. *Ore Geol. Rev.* **2016**, *79*, 332–345. [CrossRef]
7. Cheng, Y.B.; Mao, J.W. Age and geochemistry of granites in Gejiu area, Yunnan province, SW China: Constraints on their petrogenesis and corresponding tectonic setting. *Lithos* **2010**, *120*, 258–276. [CrossRef]
8. Zhao, Z.Y.; Hou, L.; Ding, J.; Zhang, Q.M.; Wu, S.Y. A genetic link between Late Cretaceous granitic magmatism and Sn mineralization in the southwestern South China Block: A case study of the Dulong Sn-dominant polymetallic deposit. *Ore Geol. Rev.* **2018**, *93*, 268–289. [CrossRef]
9. Zhang, H.; Gao, Z.M.; Ma, D.Y.; Tao, Y. Pb isotopic compositions and its significance in ore genesis in Gejiu tin-polymetallic deposits. *Acta Mineral. Sin.* **2004**, *24*, 149–152, (In Chinese with English abstract).
10. Zhang, Y.H.; Zhang, S.T. Geochemical characteristics of granite in the Guanfang tungsten deposit of Wenshan, Yunnan Province and its geological implications. *Geol. Explor.* **2011**, *47*, 1002–1008, (In Chinese with English abstract).
11. Cherniak, D.J.; Watson, E.B.; Grove, M.; Harrison, T.M. Pb diffusion in monazite: A combined RBS/SIMS study. *Geochim. Cosmochim. Acta* **2004**, *68*, 829–840. [CrossRef]
12. Foster, G.; Kinney, P.; Vance, D.; Prince, C.; Harris, N. The significance of monazite U-Th-Pb age data in metamorphic assemblages; a combined study of monazite and garnet chronometry. *Earth Planet. Sci. Lett.* **2000**, *181*, 327–340. [CrossRef]
13. Catlos, E.J.; Gilley, L.D.; Harrison, T.M. Interpretation of monazite ages obtained via in situ analysis. *Chem. Geol.* **2002**, *188*, 193–215. [CrossRef]
14. Smith, H.A.; Giletti, B.J. Lead diffusion in monazite. *Geochim. Cosmochim. Acta* **1997**, *61*, 1047–1055. [CrossRef]
15. Meldrum, A.; Boatner, L.A.; Weber, W.J.; Ewing, R.C. Radiation damage in zircon and monazite-radiation dose-dependent structural characteristics. *Geochim. Cosmochim. Acta* **1998**, *62*, 2509–2520. [CrossRef]
16. Suzuki, K.; Adachi, M.; Kajizuka, I. Electron microprobe observations of Pb diffusion in metamorphosed detrital monazites. *Earth Planet. Sci. Lett.* **1994**, *128*, 391–405. [CrossRef]
17. Chappell, B.W.; White, A.J.R. Two contrasting granite types: 25 years later. *Aust. J. Earth Sci.* **2001**, *48*, 489–499. [CrossRef]

18. Alagna, K.E.; Petreli, M.; Perugini, D.; Poli, D. Micro-analytical zircon and monazite U-Pb isotope dating by laser ablation-inductively coupled plasma-quadrupole mass spectrometry. *Geostand. Geoanal. Res.* **2008**, *32*, 103–120. [CrossRef]
19. Li, J.D. Geochemistry, Zircon U-Pb Geochronology and Implication for Tectonic Setting of the Bozhushan Granite in Southeastern Yunnan Province, SW China. Master Thesis, China University of Geosciences, Beijing, China, 2018. (In Chinese with English abstract).
20. Ouyang, Y.P. Diversity of Mineralization and Spectrum of Tungsten-Tin Polymetallic Deposits in Southeastern Yunnan Province, China. Master Thesis, China University of Geosciences, Wuhan, China, 2013. (In Chinese with English abstract).
21. Li, K.W.; Zhang, Q.; Wang, D.P.; Cai, Y.; Liu, Y.P. LA-MC-ICP-MS U-Pb geochronology of cassiterite from the Bainiuchang polymetallic Deposit, Yunnan Province, China. *Acta Mineral. Sin.* **2013**, *33*, 203–209, (In Chinese with English abstract).
22. Zhang, H.P.; Liu, J.S.; Li, X.B.; Zhang, X.L. Relationship of granites to tin, silver, copper, lead, zinc, polymetallic deposits in southeastern Yunnan, China. *Contrib. Geol. Miner. Resour. Res.* **2006**, *21*, 87–90, (In Chinese with English abstract).
23. Zhang, Q.; Li, K.W.; Wang, D.P.; Hou, X.F. New geological and geochemical evidence of Bainiuchang polymetallic deposit in southeastern Yunnan. *Acta Miner. Sin.* **2009**, *29*, 355–356, (In Chinese with English abstract).
24. Zhang, H.P. Bainiuchang Sliver Polymetallic Deposit in Mengzi, Yunnan Province: A Granite-related Supergiant Deposit. PhD Thesis, Centrl South University, Changsha, China, 2007. (In Chinese with English abstract).
25. Chen, X.C.; Hu, R.Z.; Bi, X.W.; Zhong, H.; Lan, J.B.; Zhao, C.H.; Zhu, J.J. Zircon U–Pb ages and Hf–O isotopes, and whole-rock Sr–Nd isotopes of the Bozhushan granite, Yunnan province, SW China: Constraints on petrogenesis and tectonic setting. *J. Asian Earth Sci.* **2015**, *99*, 57–71. [CrossRef]
26. Zong, K.Q.; Klemd, R.; Yuan, Y.; He, Z.Y.; Guo, J.L.; Shi, X.L.; Liu, Y.S.; Hu, Z.C.; Zhang, Z.M. The assembly of Rodinia: The correlation of early Neoproterozoic (ca.900Ma) high-grade metamorphism and continental arc formation in the southern Beishan Orogen, southern Central Asian Orogenic Belt (CAOB). *Precambrian Res.* **2017**, *290*, 32–48. [CrossRef]
27. Wiedenbeck, M.; Hanchar, J.M.; Peck, W.H.; Sylvester, P.; Valley, J.; Whitehouse, M.; Franchi, I. Further characterisation of the 91500 zircon crystal. *Geostand. Geoanal. Res.* **2004**, *28*, 9–39. [CrossRef]
28. Wiedenbeck, M.; Alle, P.; Corfu, F.; Griffin, W.L.; Meier, M.; Oberli, F.V.; Von Quadt, A.; Roddick, J.C.; Spiegel, W. Three natural zircon standards for U-Th-Pb, Lu-Hf, trace element and REE analyses. *Geostand. Newslett.* **1995**, *19*, 1–23. [CrossRef]
29. Liu, Y.S.; Hu, Z.C.; Gao, S.; Günther, D.; Xu, J.; Gao, C.G.; Chen, H.H. In situ analysis of major and trace elements of anhydrous minerals by LA-ICP-MS without applying an internal standard. *Chem. Geol.* **2008**, *257*, 34–43. [CrossRef]
30. Liu, Y.S.; Gao, S.; Hu, Z.C.; Gao, C.G.; Zong, K.Q.; Wang, D.B. Continental and oceanic crust recycling-induced melt-peridotite interactions in the Trans-North China Orogen: U-Pb dating, Hf isotopes and trace elements in zircons of mantle xenoliths. *J. Petrol.* **2010**, *51*, 537–571. [CrossRef]
31. Ludwig, K.R. *ISOPLOT 3.00: A Geochronological Toolkit for Microsoft Excel*; Special Publication/Berkeley Geochronology Center: Berkeley, CA, USA, 2003; Volume 4, pp. 1–71.
32. Anderson, T. Correction of common lead in U-Pb analyses that do not report $^{204}$Pb. *Chem. Geol.* **2002**, *192*, 59–79. [CrossRef]
33. Hu, Z.C.; Zhang, W.; Liu, Y.S.; Hu, Z.C.; Zhang, W.; Liu, Y.S.; Gao, S.; Li, M.; Zong, K.Q.; Chen, H.H.; et al. "Wave" signal smoothing and mercury removing device for laser ablation quadrupole and multiple collector ICP-MS analysis: Application to lead isotope analysis. *Anal. Chem.* **2015**, *87*, 1152–1157. [CrossRef]
34. Zong, K.Q.; Chen, J.Y.; Hu, Z.C.; Liu, Y.S.; Li, M.; Fan, H.H.; Meng, Y.N. In-situ U-Pb dating of uraninite by fs-LA-ICP-MS. *Sci. China Earth Sci.* **2015**, *58*, 1731–1740. [CrossRef]
35. Aleinikoff, J.N.; Schenck, W.S.; Plank, M.O.; Srogi, L.; Fanning, C.M.; Kamo, S.L. Deciphering igneous and metamorphic events in high grade rocks of the Wilmington Complex, Delaware: Morphology, cathodoluminescence and backscattered electron zoning, and SHRIMP U-Pb geochronology of zircon and monazite. *Geol. Soc. Am. Bull.* **2006**, *118*, 39–64. [CrossRef]

36. Tomascak, P.B.; Krogstad, E.J.; Walker, R.J. U-Pb monazite geochronology of granitic rocks from Maine: Implications for Late Paleozoic tectonics in the northern Appalachians. *J. Geol.* **1996**, *104*, 185–195. [CrossRef]
37. Hoskin, P.W.O.; Black, L.P. Metamorphic zircon formation by solid: Tate recrystallization of protolith igneous zircon. *J. Metamorph. Geol.* **2001**, *18*, 423–439. [CrossRef]
38. Taylor, S.R.; McLennan, S.M. *The Continental Crust: Its Composition and Evolution*; Blackwell Scientific Publications: Oxford, UK, 1985; pp. 1–312.
39. Blevin, P.L. Redox and compositional parameters for interpreting the granite metallogeny of Eastern Australia: Implications for gold-rich ore system. *Resour. Geol.* **2004**, *54*, 241–252. [CrossRef]
40. Cheng, Y.B.; Mao, J.W.; Chang, Z.; Pirajno, F. The origin of the world class tin-polymetallic deposits in the Gejiu district, SW China: Constraints from metal zoning characteristics and 40Ar–39Ar geochronology. *Ore Geol. Rev.* **2013**, *53*, 50–62. [CrossRef]
41. Cheng, Y.B.; Mao, J.W.; Spandler, C. Petrogenesis and geodynamic implications of the Gejiu igneous complex in the western Cathaysia block, South China. *Lithos* **2013**, *175–176*, 213–229. [CrossRef]
42. Liu, Y.P.; Li, Z.X.; Li, H.M. U-Pb geochronology of cassiterite and zircon from the Dulong Sn-Zn deposit: Evidence for Cretaceous large-scale granitic magmatism and mineralization events in southeastern Yunnan province. *China. Acta Petrol. Sin.* **2007**, *23*, 967–976, (In Chinese with English abstract).
43. Feng, J.R.; Mao, J.W.; Pei, R.F. Ages and geochemistry of Laojunshan granites in southeastern Yunnan, China: Implications for Sn-W polymetallic ore deposits. *Mineral. Petrol.* **2013**, *107*, 573–589. [CrossRef]